



HAL
open science

Tunable microwave impedance matching to a high impedance source using a Josephson metamaterial

Carles Altimiras, Olivier Parlavecchio, Philippe Joyez, Denis Vion, Patrice Roche, Daniel Esteve, Fabien Portier

► **To cite this version:**

Carles Altimiras, Olivier Parlavecchio, Philippe Joyez, Denis Vion, Patrice Roche, et al.. Tunable microwave impedance matching to a high impedance source using a Josephson metamaterial. Applied Physics Letters, 2013, 103, pp.212601. 10.1063/1.4832074 . cea-01479016

HAL Id: cea-01479016

<https://cea.hal.science/cea-01479016>

Submitted on 28 Feb 2017

HAL is a multi-disciplinary open access archive for the deposit and dissemination of scientific research documents, whether they are published or not. The documents may come from teaching and research institutions in France or abroad, or from public or private research centers.

L'archive ouverte pluridisciplinaire **HAL**, est destinée au dépôt et à la diffusion de documents scientifiques de niveau recherche, publiés ou non, émanant des établissements d'enseignement et de recherche français ou étrangers, des laboratoires publics ou privés.

Tunable microwave impedance matching to a high impedance source using a Josephson metamaterial

Carles Altimiras,* Olivier Parlavecchio, Philippe Joyez, Denis Vion, Patrice Roche, Daniel Esteve, and Fabien Portier
*Service de Physique de l'Etat Condensé (CNRS URA 2464),
IRAMIS, CEA Saclay, 91191 Gif-sur-Yvette, France*

(Dated: April 8, 2014)

Abstract

We report the efficient coupling of a 50Ω microwave circuit to a high impedance conductor. We use an impedance transformer consisting of a $\lambda/4$ co-planar resonator whose inner conductor contains an array of superconducting quantum interference devices (SQUIDs), providing the resonator with a large and tunable lineic inductance $\mathcal{L} \sim 80\mu_0$, resulting in a large characteristic impedance $Z_C \sim 1\text{ k}\Omega$. The impedance matching efficiency is characterized by measuring the shot noise power emitted by a dc biased high resistance tunnel junction connected to the resonator. We demonstrate matching to impedances in the 15 to 35 k Ω range with bandwidths above 100 MHz around a resonant frequency tunable in the 4 to 6 GHz range.

PACS numbers: 07.57.-c, 84.37.+q, 84.40.Az, 84.40.Dc, 85.25.Dq

* carles.altimiras@sns.it; Present address: NEST, Istituto Nanoscienze CNR and Scuola Normale Superiore, Piazza San Silvestro 12, 56127, Pisa, Italy

In an electrical circuit, the output impedance of a source must be matched to the input impedance of the load in order to maximize power transfer[1]. In RF circuits, where $50\ \Omega$ matching is standard, it is difficult to detect small signals emitted from high output impedance sources. For quantum conductors, whose output impedance is typically on the order of the resistance quantum, $R_K = h/e^2 \simeq 25.8\ \text{k}\Omega$, matching is especially difficult.

Developing techniques to solve this mismatch is technologically important since high output impedance quantum circuits are promising as ultra sensitive detectors of charge, e.g. Single Electron Transistors (SETs) [2–4], or magnetic flux, e.g. Superconducting Quantum Interference Proximity Transistors (SQUIPs) [5, 6]. In both cases, their high output impedance ($\sim 100\ \text{k}\Omega$) and a typical $100\ \text{pF}$ stray capacitance to ground of the wiring limit the detection bandwidth from dc to a few kHz. An efficient technique used to overcome this limitation, originally developed to efficiently measure SETs [3], consists in embedding the sensor in a RF resonant circuit, which allows matching its high output impedance to $50\ \Omega$ at a chosen frequency. Resonant RF circuits can be made using discrete lumped elements externally connected to the chip [3, 7], or defined on-chip [8] with transmission lines terminated by an adequate impedance to ground, e.g. a stub-shunted geometry[9, 10]. On-chip impedance matching has the advantage of reducing the stray capacitance, allowing to reach detection bandwidths in the $10\ \text{MHz}$ range[8–10]. Here we report on a technique which offers matching to high detection impedances (demonstrated up to $35\ \text{k}\Omega$) at a tunable frequency in the few GHz range and with bandwidth above $100\ \text{MHz}$.

As shown in Fig.1(a), we have developed $\lambda/4$ co-planar, resonators [11] whose inner conductor contains a high kinetic inductance metamaterial [12], namely a series array of superconducting quantum interference devices (SQUIDs). This increases the characteristic impedance of the resonator[13, 14] and the resulting detection impedance. Using SQUIDs instead of plain Josephson junctions allows tuning in-situ the kinetic inductance by threading a magnetic flux in the SQUID loops. The resonator matches a highly resistive normal tunnel junction with a tunnel resistance $R_T = 230\ \text{k}\Omega$ to a $50\ \Omega$ measurement line. We characterize the resonator by detecting the well known shot-noise produced when a dc voltage bias is applied to the junction.

A $Z_0 = 50\ \Omega$ load terminating a section of length l of a transmission line with characteristic impedance Z_1 and phase velocity c is transformed into an impedance depending on

the frequency ν [11]:

$$Z(\nu) = Z_1 \frac{Z_0 + jZ_1 \tan(2\pi\nu l/c)}{Z_1 + jZ_0 \tan(2\pi\nu l/c)}, \quad (1)$$

The impedance is real and equal to Z_1^2/Z_0 at resonant frequencies $\nu_n = (2n + 1)c/4l$, with n integer, thus transforming the load impedance Z_0 into a higher impedance when $Z_1 > Z_0$. For $n = 0$, l is equal to a quarter of a wavelength, hence the name of quarter wavelength transformer. Assuming $Z_1 \gg Z_0$, the real part of the impedance reads in the vicinity of ν_0 : $\text{Re}[Z(\nu)] \sim \frac{Z_1^2}{Z_0} \left(1 + \left(\frac{\pi Z_1(\nu - \nu_0)}{2Z_0\nu_0}\right)^2\right)^{-1}$. It is equivalent to a damped LC circuit with a resonant frequency $\nu_0 = 1/(2\pi\sqrt{LC})$, impedance $Z_{\text{Res}} = \sqrt{L/C} = 4Z_1/\pi$. The external quality factor, due to dissipation in the matched load Z_0 , is $Q = \frac{\pi}{4} \frac{Z_1}{Z_0}$. Reaching an impedance $Z(\nu_0) \simeq R_K$ requires a transmission line with $Z_1 \simeq 1 \text{ k}\Omega$. This is well beyond the values attainable with metallic co-planar transmission lines, for which Z_1 only depends logarithmically on their transverse dimensions, but is achievable with high kinetic inductance lines.

A balanced SQUID [15] consists in two identical parallel Josephson junctions closing a superconducting loop. When the inductance of the loop connecting the Josephson junctions is negligible, as here, its inductance is $L_J(\phi) = \phi_0/I_C(\phi)$ with $\phi_0 = \hbar/2e$, ϕ is the flux applied through the SQUID, and I_C the critical current of the SQUID. I_C is given by the Ambegaokar-Baratoff formula [16], $I_C = \frac{\pi\Delta|\cos(\phi/2\phi_0)|}{eR_N}$ with R_N is the tunnel resistance of each junction. This expression for the Josephson inductance is valid provided that i) the characteristic energies $h\nu$ and $k_B T$ respectively associated to the frequency and the temperature are much smaller than the superconducting gap, ii) the phase across the junction can be considered as a classical quantity[17], and iii) is much smaller than 1, which implies that the current going through the SQUID is much smaller than I_C . To evaluate the lineic impedance \mathcal{Z} of the inner conductor of our transmission line, one must take into account the capacitance C_J of the tunnel junction, yielding $\mathcal{Z} = i2\pi\nu L_J(\phi)/a(1 - \nu^2/\nu_P^2)$, with ν_P the Josephson plasma frequency[18] $\nu_P = 1/[2\pi(L_J C_J)^{1/2}]$, and a is the distance between neighbouring SQUIDs. Below ν_P , the inner conductor thus presents an effective lineic inductance

$$\mathcal{L} = L_J(\phi)/a(1 - \nu^2/\nu_P^2). \quad (2)$$

The characteristic impedance of the SQUID transmission line is then given by $Z_1 = \sqrt{\mathcal{L}/\mathcal{C}}$, where \mathcal{C} is the lineic capacitance to ground of the SQUID array, evaluated using standard

electromagnetic simulations. Note that at frequencies much lower than ν_P , \mathcal{L} is independent of frequency, so that our device can be considered as a standard quarter wavelength impedance transformer, albeit with high lineic inductance. Finally, we would like to point that this technique cannot provide characteristic impedances $Z_1 \gg R_Q$, since quantum phase slips then drive the array into an insulating state [19].

Figure 1(a) shows a picture of the measured co-planar resonator and its equivalent electric circuit scheme. From the left to the right a $50\ \Omega$ line is followed by a $350\ \mu\text{m}$ long Josephson metamaterial line containing lithographically identical and evenly spaced SQUIDs with a $5\ \mu\text{m}$ period. SQUIDs were fabricated following the process described in Ref. [20]: the SQUIDs (see the top inset) are obtained by double angle deposition of (20/40 nm) thin aluminum electrodes, with a 20' oxydation of the first electrode at 400 mBar of a (85% O_2 /15% Ar) mixture. Before the evaporation, the substrate was cleaned by rinsing in ethanol and Reactive Ion Etching in an oxygen plasma [21]. The barriers have an area of $0.5\ \mu\text{m}^2$ each resulting in a room temperature tunnel resistance $R_N = 720\ \Omega$. To assess that the SQUIDs in the array are identical, we have performed reproducibility tests, yielding constant values of R_N (within a few %) over millimetric distances. Assuming a superconducting gap $\Delta = 180\ \mu\text{eV}$ and a 17% increase of the tunnel resistance between room temperature and base temperature [22], one obtains a zero flux critical current for the SQUIDs $I_C = 671\ \text{nA}$, corresponding to $L_J(\phi = 0) = 0.49\ \text{nH}$. This corresponds to an effective lineic inductance $\mathcal{L} \simeq 100\ \mu\text{H.m}^{-1}$ at zero magnetic flux and frequency much lower than ν_P . Assuming a capacitance for the junctions of the order of $80\ \text{fF}/\mu\text{m}^2$ yields $\nu_P \simeq 25\ \text{GHz}$. Note that our simple fabrication mask (see Top Panel in Fig. 1(a)) produces 10 times bigger Josephson junction in between adjacent SQUIDs, resulting in an additional $\sim \mathcal{L} \simeq 10\ \mu\text{H.m}^{-1}$ lineic inductance. The $\sim \mathcal{L} \simeq 1\ \mu\text{H.m}^{-1}$ electromagnetic inductance associated to our geometry is negligible. With the designed lineic capacitance $\mathcal{C} = 84.3\ \text{pF.m}^{-1}$, the length of the resonator sets the first resonance at $\nu_0 \simeq 7\ \text{GHz}$ with an impedance $Z_{\text{Res}} \simeq 1.5\ \text{k}\Omega$ and quality factor $Q \simeq 18$. The frequency ν_0 being small enough compared to ν_P , the frequency dependence of \mathcal{L} given by Eq.2 is almost negligible. Sweeping the field then modifies $\mathcal{L} \propto |\cos(\phi/2\phi_0)|^{-1}$, $\nu_0 \propto |\cos(\phi/2\phi_0)|^{0.5}$, the impedance $Z_{\text{Res}} \propto |\cos(\phi/2\phi_0)|^{-0.5}$ and the quality factor $Q \propto |\cos(\phi/2\phi_0)|^{-0.5}$. The 0.35 mT field period is estimated from the $3\ \mu\text{m}^2$ SQUID area.

The $100 \times 100\ \text{nm}^2$ normal tunnel junction (see Fig. 1(a) bottom inset) is fabricated

by multiple angle evaporation of copper/aluminum/copper with thicknesses (30/5/60 nm), and a 20' oxydation of aluminum at 800 mBar of a (85% O₂/15% Ar) mixture. Using the standard theory of the proximity effect [23], we find that the aluminum superconductivity is fully suppressed in the lower electrode. Finally a $30 \times 50 \times 0.3 \mu\text{m}^3$ normal metal (gold) pad is inserted between the SQUID array and the normal junction, in order to efficiently absorb the power dissipated at the biased normal tunnel junction. The electron-phonon coupling [24, 25] is sufficient to maintain the electronic temperature below ~ 20 mK at the maximum bias voltage used here. For the same reason, the ground plane is also made of $0.3 \mu\text{m}$ thick gold. This pad adds an extra capacitance to ground $C_{\text{shunt}} \simeq 12$ fF (estimated numerically). The impedance across the tunnel junction $Z(\nu)$ is the parallel combination of C_{shunt} and the 50Ω load transformed by the quarter wavelength section. As seen from the junction, the main effect of this capacitance is thus to reduce the resonant frequency and the associated impedance ($\nu_0 \simeq 6$ GHz and $Z_{\text{Res}} \simeq 1$ k Ω at zero flux).

A schematic diagram of the measuring set-up is shown in Fig. 1(b). The device is cooled in a dilution fridge with a $T = 15$ mK base temperature. The device is connected to the measurement circuit through a 50Ω matched commercial bias Tee. Its inductive port is used to current bias the normal tunnel junction via a $13 \text{ M}\Omega$ resistor anchored at 0.8 K. The resulting dc voltage across the sample is measured in a 3 point configuration via a room temperature commercial voltage pre-amplifier, which allows an in-situ measurement of the voltage across the device, from which we deduce R_{T} . The dc lines are carefully filtered by custom made passive filters (a 3rd order RC filter with $R = 2$ k Ω , $C = 1$ nF anchored at 0.8 K, followed by a 170Ω , 450 pF distributed RC filter and a bronze powder filter, both anchored at base temperature).

The capacitive port of the bias Tee couples the sample to two RF lines through a 20 dB directional coupler, whose direct port couples the sample to the detection chain. This chain consists of a $4 - 8$ GHz isolator, a $4 - 8$ GHz band pass filter, a low pass dissipative gaussian filter (-3 dB at 12 GHz), and a 40 dB gain cryogenic amplifier with 3.5 K noise temperature. The rejection noise of the amplifier is routed by the isolator to a 50Ω load anchored at the base temperature. The amplified signal is then measured at room temperature via an active circuit equivalent to 15 MHz band-pass filter around an adjustable frequency ν . This is performed by heterodyning the signal with an external local oscillator using a mixer, and passing the down-converted signal through a low-pass filter. The signal is then fed to a 50Ω

matched square-law detector whose output dc voltage is proportional to the incoming RF power. Since the resulting signal contains a small contribution from the sample on top of the much larger noise of the cryogenic amplifier, a standard Lock-in technique is used by adding a small ac bias to the normal tunnel junction with a near dc frequency (~ 15 Hz) and measuring the response of the square law detector in phase with the excitation. The gain of the detection chain $G(\nu)$ is calibrated in-situ by exploiting the feed line coupled to the sample via the -20 dB port of the directional coupler. This feed line contains 70 dB attenuation distributed in 3 stages thermally anchored at progressively lower temperatures, a low pass dissipative gaussian filter (-3 dB at 12 GHz), and a 4 – 8 GHz bandpass filter, which, altogether with the directional coupler, have been independently calibrated at 4.2 K. The feed this line is connected to a synthesizer with a level ~ 1 dBm.

By setting the device resonance frequency below 4 GHz, the entire power incoming from the feed line is reflected by the device, which allows to calibrate the detection chain in the 4-7 GHz frequency range used in the experiments described below. One has to correct for the double passage through the bias Tee and the 10 cm coaxial cable connecting it to the sample, both independently calibrated. With this calibration in hand, we characterize the resonator with the on-chip radiation source provided by the electronic shot-noise of the tunnel junction. Indeed, at large dc bias voltage $eV \gg k_B T, h\nu$, a biased tunnel junction is a source of white current noise with a power spectral density $S_I = 2eV/R_T$. The power density delivered to the 50Ω chain reads

$$P(\nu) = \frac{2eV \text{Re}[Z(\nu)] R_T}{|Z(\nu) + R_T|^2} \simeq \frac{2eV \text{Re}[Z(\nu)] R_T}{(\text{Re}[Z(\nu)] + R_T)^2}, \quad (3)$$

where the last approximation holds if $\text{Im}[Z(\nu)] \ll R_T$. This approximation, which allows to extract $\text{Re}[Z(\nu)]$ from $P(\nu)$, results in a less than 2% error, smaller than the $\sim 1 - 2$ dB uncertainty in the gain calibration.

The impedance $\text{Re}[Z(\nu, \phi)]$ extracted in this manner is shown in the right panel of Fig.2, next to the values predicted without fitting parameter. Besides a spurious resonance at 5.8 GHz, the data mostly present the expected resonance at frequency $\nu_0 |\cos(\phi/2\phi_0)|^{0.5}$ with $\nu_0 = 6$ GHz, and reach detection impedances always above 10 k Ω .

In order to analyze more quantitatively the impedance matching capability of our device and its comparison to the model, several curves obtained for distinct external magnetic fields are shown in Fig.3 and compared to the predictions. These data show a variation of the

bandwidth in the 100 to 240 MHz range, and of the detection impedance in the 15 to 35 k Ω range, as predicted. The 15% agreement obtained for the impedance is compatible with our gain calibration uncertainty 1 – 2 dB.

Beyond an increased coupling to high output impedance sensors, the resonators developed here enrich the toolbox of quantum electrical engineering, in particular for circuit cavity quantum electrodynamics. Indeed, higher characteristic impedances would increase the coupling of double quantum dot qubits to the microwave cavity in which they are embedded [26, 27], helping to reach the strong coupling regime. They could also be used to probe Kondo physics with microwave photons [28, 29].

Being based on well known technology, it is fairly simple to predict the response of our devices as long as their Josephson junctions remain in the linear regime, which implies that the current must be kept well below their critical current. Note that when approaching the Josephson plasma frequency (~ 25 GHz for aluminum based junctions), this strongly reduces the corresponding maximum microwave power. Above the Josephson plasma frequency, the capacitance of the junctions shunts their kinetic inductance, and the basic mechanism of our technique breaks down. This physical limit can however be easily pushed up by using higher gap material, e.g. niobium nitride for which plasma frequencies above a few 100 GHz have been demonstrated [30, 31]. Other schemes could also be implemented to bypass this limit, such as using thin films of highly disordered superconductors [32] which have a large kinetic inductance, or superconductor-normal metal-superconductor weak links [33] which furthermore have a negligible inter-electrode capacitance.

In conclusion, we have demonstrated impedance matching to 50 Ω of a high impedance component using a microwave resonator embedding a Josephson metamaterial that yields a large resonator impedance. The matching frequency is tunable in the 4 and 6 GHz range, with the bandwidth varying from ~ 100 to 240 MHz. This impedance matching has been characterized using an on-chip white noise source. This method offers interesting perspectives for quantum electrical engineering at even larger frequency and impedance values.

This project was funded by the CNano-IDF Shot-E-Phot, the Triangle de la Physique DyCoBloS and ANR AnPhoTeQ and Masquel grants. Technical assistance from Patrice

Jacques, Pierre-Francois Orfila and Pascal Sénat are gratefully acknowledged.

- [1] P. Horowitz and W. Hill, *The Art of Electronics*, 2nd ed. (Cambridge University Press, New York, 1989).
- [2] T. A. Fulton and G. J. Dolan, *Phys. Rev. Lett.* **59**, 109 (1987).
- [3] R. J. Schoelkopf, P. Wahlgren, A. A. Kozhevnikov, P. Delsing, and D. E. Prober, *Science* **280**, 1238 (1998).
- [4] A. Aassime, D. Gunnarsson, K. Bladh, P. Delsing, and R. Schoelkopf, *Applied Physics Letters* **79**, 4031 (2001).
- [5] F. Giazotto, J. T. Peltonen, M. Meschke, and J. P. Pekola, *Nature Phys.* , 254 (2010).
- [6] F. Giazotto and F. Taddei, *Phys. Rev. B* **84**, 214502 (2011).
- [7] T. Müller, B. Küng, S. Hellmüller, P. Studerus, K. Ensslin, T. Ihn, M. Reinwald, and W. Wegscheider, *Applied Physics Letters* **97**, 202104 (2010).
- [8] W. W. Xue, B. Davis, F. Pan, J. Stettenheim, T. J. Gilheart, A. J. Rimberg, and Z. Ji, *Applied Physics Letters* **91**, 093511 (2007).
- [9] S. Hellmüller, M. Pikulski, T. Müller, B. Küng, G. Puebla-Hellmann, A. Wallraff, M. Beck, K. Ensslin, and T. Ihn, *Applied Physics Letters* **101**, 042112 (2012).
- [10] G. Puebla-Hellmann and A. Wallraff, *Applied Physics Letters* **101**, 053108 (2012).
- [11] D. M. Pozar, *Microwave Engineering*, 4th ed. (John Wiley and Sons Inc., New York, 2011).
- [12] M. A. Castellanos-Beltran and K. W. Lehnert, *Applied Physics Letters* **91**, 083509 (2007).
- [13] N. A. Masluk, I. M. Pop, A. Kamal, Z. K. Mineev, and M. H. Devoret, *Phys. Rev. Lett.* **109**, 137002 (2012).
- [14] M. T. Bell, I. A. Sadovskyy, L. B. Ioffe, A. Y. Kitaev, and M. E. Gershenson, *Phys. Rev. Lett.* **109**, 137003 (2012).
- [15] R. C. Jaklevic, J. Lambe, A. H. Silver, and J. E. Mercereau, *Phys. Rev. Lett.* **12**, 159 (1964).
- [16] V. Ambegaokar and A. Baratoff, *Phys. Rev. Lett.* **10**, 486 (1963).
- [17] P. Joyez, *Phys. Rev. Lett.* **110**, 217003 (2013).
- [18] B. D. Josephson, *Rev. Mod. Phys.* **36**, 216 (1964).
- [19] E. Chow, P. Delsing, and D. B. Haviland, *Phys. Rev. Lett.* **81**, 204 (1998).

- [20] I. M. Pop, T. Fournier, T. Crozes, F. Lecocq, I. Matei, B. Pannetier, O. Buisson, and W. Guichard, *Journal of Vacuum Science Technology B: Microelectronics and Nanometer Structures* **30**, 010607 (2012), arXiv:1105.6204 [cond-mat.mes-hall].
- [21] Following Ref.²⁰, we performed Reactive Ion Etching under an oxygen pressure of 30 mBar and 10 W RF power, during 15 seconds, in a Plassys MG -200- S RIE equipment.
- [22] K. Gloos, R. S. Poikolainen, and J. P. Pekola, *Applied Physics Letters* **77**, 2915 (2000).
- [23] P. G. de Gennes, *Rev. Mod. Phys.* **36**, 225 (1964).
- [24] B. Huard, H. Pothier, D. Esteve, and K. E. Nagaev, *Phys. Rev. B* **76**, 165426 (2007).
- [25] F. Giazotto, T. T. Heikkilä, A. Luukanen, A. M. Savin, and J. P. Pekola, *Rev. Mod. Phys.* **78**, 217 (2006).
- [26] M. R. Delbecq, V. Schmitt, F. D. Parmentier, N. Roch, J. J. Viennot, G. Fève, B. Huard, C. Mora, A. Cottet, and T. Kontos, *Phys. Rev. Lett.* **107**, 256804 (2011).
- [27] T. Frey, P. J. Leek, M. Beck, A. Blais, T. Ihn, K. Ensslin, and A. Wallraff, *Phys. Rev. Lett.* **108**, 046807 (2012).
- [28] K. Le Hur, *Phys. Rev. B* **85**, 140506 (2012).
- [29] M. Goldstein, M. H. Devoret, M. Houzet, and L. I. Glazman, *Phys. Rev. Lett.* **110**, 017002 (2013).
- [30] J.-C. Villgier, B. Delaet, V. Larrey, M. Salez, Y. Delorme, and J.-M. Munier, *Applied Superconductivity* **6**, 541 (1999).
- [31] Y. Nagai, H. Akaike, R. Kanada, N. Naito, and A. Fujimaki, *Superconductor Science and Technology* **22**, 114015 (2009).
- [32] E. F. C. Driessen, P. C. J. J. Coumou, R. R. Tromp, P. J. de Visser, and T. M. Klapwijk, *Phys. Rev. Lett.* **109**, 107003 (2012).
- [33] J. Clarke, *Phys. Rev. B* **4**, 2963 (1971)

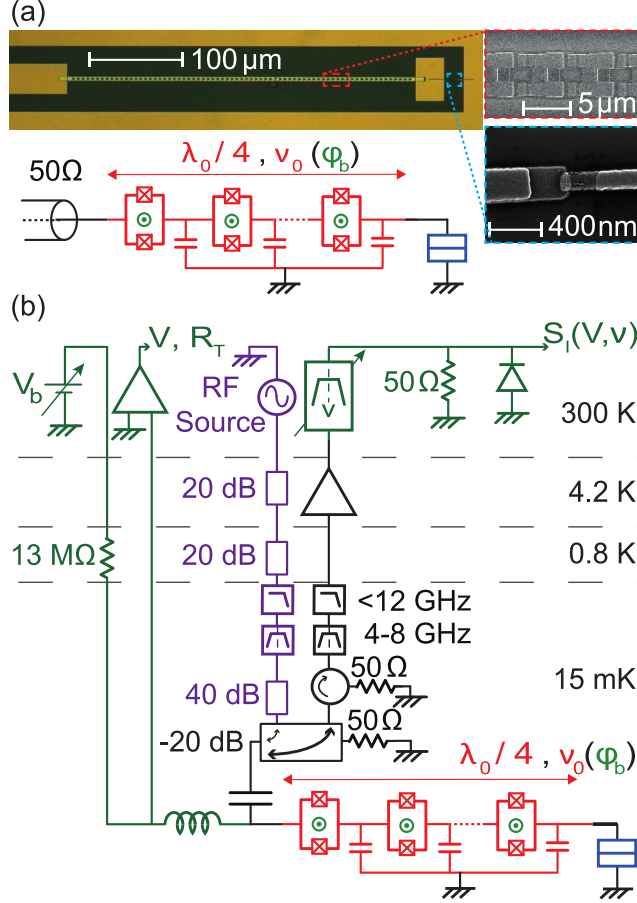


FIG. 1. (Color online) **Description of the device and characterization circuit.** (a) Optical microscope image of the $\lambda/4$ co-planar resonator based on a Josephson metamaterial, on top of the scheme of its equivalent electric circuit. Top inset: scanning electron microscope (SEM) image of few SQUIDs from the Josephson metamaterial. Bottom inset: SEM image of the high resistance normal tunnel junction terminating the resonator. (b) Electric circuit used to characterize the resonator: The sample shown in (a) is connected to the circuit with a bias tee. The inductive port is used to dc bias the sample and to measure the normal state resistance of the tunnel junction in a three point configuration. The capacitive port is used to amplify, filter and measure the fraction of the RF power emitted by the tunnel junction which is transmitted by the resonator. This quantity depends only on the dc bias, the detection impedance provided by the resonator, the output impedance of the tunnel junction and the gain of the detection chain. An additional RF line, heavily attenuated and connected to the circuit via a -20dB directional coupler, is used to calibrate the gain of the detection chain. For this calibration, the resonant frequency of the resonator is tuned out of the detection bandwidth so that the incoming radiation is fully reflected by the sample.

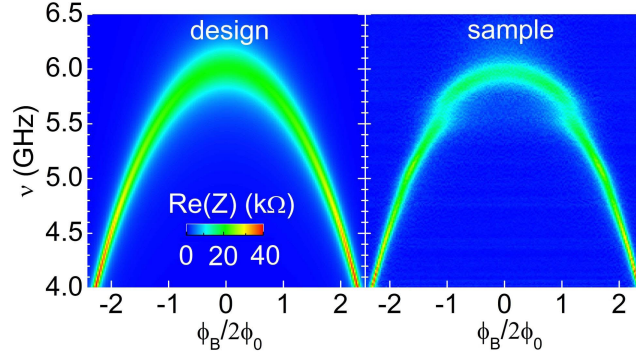


FIG. 2. (Color online) Left panel: predicted real part of the detection impedance $\text{Re}[Z(\nu, \phi)]$ obtained by terminating the resonator with a $50\ \Omega$ load as a function of frequency ν and the externally applied magnetic flux ϕ . Right panel: $\text{Re}[Z(\nu, \phi)]$ obtained experimentally. The dc biased tunnel junction is used as an on-chip calibrated RF source feeding the resonator with white current noise. The fraction of RF power transmitted by the resonator depends only on the dc bias, the detection impedance provided by the resonator, the output impedance of the tunnel junction and the gain of the detection chain allowing to extract $\text{Re}[Z(\nu, \phi)]$ with Eq. (3).

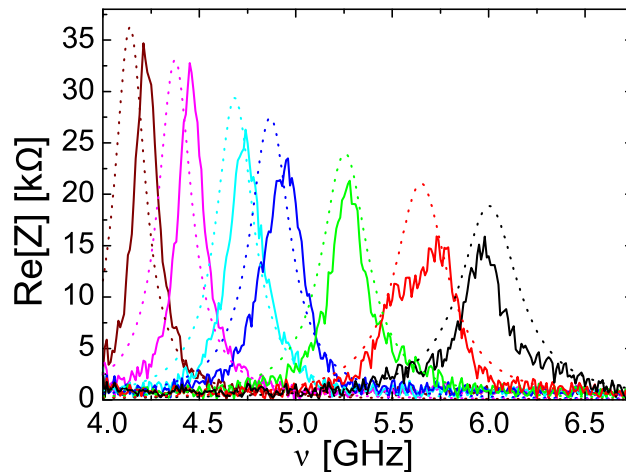


FIG. 3. (Color online) Comparison between the measured (full lines) and the predicted (dotted lines) $\text{Re}[Z_{\text{det}}(\nu, \phi)]$ for several values of the externally applied magnetic flux $\phi = (0, 0.16, 0.23, 0.28, 0.3, 0.33, 0.35)$ from the left to the right.